JAAS

ROYAL SOCIETY OF CHEMISTRY

PAPER

View Article Online
View Journal

Cite this: DOI: 10.1039/d5ja00513b

Determination of REEs in permanent magnets and their production chain using ICP-MS

Laura Suárez-Criado, [a] Cyril Rado, [b] Delphine Losno [ac] and Frank Vanhaecke *[a]

This paper presents the development, optimization and use of a method for the determination of the rare earth elements (REEs) in Nd–Fe–B permanent magnets and samples from their production chain. This analytical method was developed for the purpose of contributing to the transparency, traceability, and sustainability of complex supply chains of critical raw materials, such as REEs. The approach developed combines acid extraction of the REEs, chromatographic separation using commercially available AG® MP-1M anionic resin and LN specific resin (100–150 μm) and ICP-MS analysis for their subsequent quantitative determination. Physical separation (chromatography) proved essential to overcome interference from polyatomic ions, enabling accurate quantification despite the occurrence of oxide and hydroxide ions of heavier REEs otherwise interfering with the determination of some lighter REEs due to unfavorable elemental ratios. The high iron content of magnet samples negatively affected the elution profile of light REEs from LN specific resin, necessitating prior Fe removal using AG® MP-1M resin. The reliability of the method was evaluated using the USGS BHVO-2 reference material. Distinct REE patterns were observed among magnet samples, while samples from the production chain showed some small variations only.

Received 23rd December 2025
Accepted 3rd March 2026

DOI: 10.1039/d5ja00513b

rsc.li/jaas

1. Introduction

Rare earth elements (REEs) are a group of 17 elements consisting of the lanthanides (Ln), together with scandium (Sc) and yttrium (Y), which are attracting increasing attention due to their exponential demand in the high-tech industry.[1] If Sc is excluded because of its distinct chemistry, REEs can be divided into two groups: light REEs (LREEs), ranging from lanthanum (La) to gadolinium (Gd), and heavy REEs (HREEs), covering the range from terbium (Tb) to lutetium (Lu) plus Y.[2] Considered critical raw materials (CRMs), REEs are crucially important in the renewable energy sector, where praseodymium (Pr), neodymium (Nd), and dysprosium (Dy) play a key role as essential components in the production of neodymium–iron–boron (Nd–Fe–B) permanent magnets, used in high-performance wind turbines and electric vehicle traction motors.[3]

Contrary to what their name suggests, REEs are relatively abundant in the Earth's crust, with global reserves estimated at approximately 130 million tons.[4] However, they are present in the form of minerals such as monazite, bastnaesite, or xenotime, making their extraction difficult and costly.[5] China dominates the world's REE reserves, holding over 30% of the global LREE deposits,[6] with the Bayan Obo mine, the world's largest REE mine, as a notable example. Outside China, the main LREE mines are Mountain Pass in the USA and Mount Held in Australia; in Europe, there are no active mines, only several exploration targets, mostly located in the northern countries.[7] Illegal mining activity, however, mostly of HREEs, is taking place in conflict areas such as the Myanmar/China border area.[8]

Once extracted from the ore, REEs undergo physicochemical refinement to obtain REE concentrates, which are then processed into intermediate compounds such as carbonates, oxides, and oxalates. Subsequently, the REEs are separated from one another and individually refined, and ultimately alloyed with other metals/metalloids, for instance with Fe and B[9] to produce permanent magnets. It is estimated that China's annual production of Nd–Fe–B permanent magnets accounts for between 85 and 90% of the global total, a figure that continues to grow.[10] Currently, Europe[11] depends completely on Chinese supply and China is restricting the export of REEs and magnets.

Ensuring a sustainable supply of minerals and metals required for the production of renewable energy, especially that of critical elements like REEs, is crucial to preventing a future mineral crisis. To support this, establishing effective and efficient traceability systems is imperative,[12] requiring the capability for analysis of raw materials and products throughout the production chain, among other actions. In general, REEs are valuable for fingerprinting purposes due to their low natural

[a]Ghent University, Department of Chemistry, Atomic & Mass Spectrometry – A&MS Research Unit, Campus Sterre – Building S12, De Pintelaan 270, 9000 Ghent, Belgium. E-mail: Frank.Vanhaecke@UGent.be
[b]Univ. Grenoble Alpes, CEA LITEN, Grenoble 38000, France
[c]BRGM, F-45060 Orléans, France

geochemical concentrations and distinct element-content patterns in rocks, known as REE-patterns.[13] Present-day analytical protocols enable the detection of even slight variations in their concentrations within any geological system, providing a robust tool for tracing material provenance and understanding geological processes.[14] However, the use of REEs as fingerprinting tracers in permanent magnets linking these final products to the raw material used in their manufacturing is challenged by the impact of various stages of the metallurgical production chain.

For the determination of REEs, techniques such as Inductively Coupled Plasma-Optical Emission Spectrometry (ICP-OES), Neutron Activation Analysis (NAA) and X-ray fluorescence spectrometry (XRF) can be used, although Inductively Coupled Plasma-Mass Spectrometry (ICP-MS) is the most powerful technique due to its high sensitivity, multi-element capabilities, and wide linear dynamic range, among other advantages.[15] Nevertheless, careful attention must be paid to adequate selection of the instrument settings and validation of the data quality, as both isobaric and polyatomic ions can interfere with the determination of REEs, potentially leading to erroneous concentration values.[16] While all lanthanides have at least one isotope free from isobaric interference, oxide and hydroxide ions formed by lighter REEs in the plasma may show the same nominal mass-to-charge (m/z) ratio as nuclides of Gd and HREEs.[17] These polyatomic interferences particularly jeopardize the accuracy of the results when the concentration of the LREE at the origin of a (hydr)oxide ion is high relative to that of the HREE affected by that ion, as is commonly the case in Nd–Fe–B permanent magnets (*e.g.*, Nd and Pr together account for more than 30% of the total mass).

As a solution to the problem of interference, the use of an ICP-MS instrument equipped with a collision/reaction cell (CRC) or with a double-focusing sector field mass spectrometer that can be operated at higher mass resolution can be considered.[18] However, the use of a CRC can reduce oxide formation but not fully eliminate it,[19] while the maximum mass resolution of state-of-the-art high-resolution ICP-MS instruments is below that required for successfully addressing the aforementioned spectral overlap.[20] Increase of the mass resolution also comes at the cost of a significant reduction in sensitivity, further challenging REE determination at (ultra)trace levels. Another option is to apply mathematical corrections, but when element ratios are unfavorable (high concentration of the interfering ion's parent nuclide *vs.* the targeted analyte nuclide) and highly reliable data are required, physical separation is typically the most reliable solution.[21] Among the separation techniques, there are on-line methods such as high-pressure ion chromatography (HPIC) or ion exchange chromatography (IEC), as well as off-line methods like precipitation/coprecipitation, liquid–liquid extraction (LLE), or solid phase extraction (SPE).[22] Of the chromatographic resins available for REE extraction, the LN resin (Eichrom Technologies) is considered the most suitable for separation of the lanthanides, with separation based on (i) an increasing charge-to-size ratio across the lanthanide series due to lanthanide contraction, and (ii) the competition between Ln^{3+} and H^+ ions for the active sites on the resin. As a result, lanthanides elute in diluted nitric acid (HNO_3) or hydrochloric acid (HCl), with the heavy lanthanides eluting at higher acid concentrations (*e.g.*, >6 M).[23]

In this work, a method for the extraction of REEs from Nd–Fe–B permanent magnets and samples from their production chain and their subsequent separation was developed using a combination of AG® MP-1M anion exchange resin and LN resin. ICP-MS was relied on for their subsequent determination. Mathematical correction for interferences due to the occurrence of oxide and hydroxide ions was tested to evaluate its applicability and limitations in case of large concentration disparities amongst the REEs, with a particular focus on Nd. The mass of LN resin and the HNO_3 gradient to be used were evaluated for the specific case of permanent magnets. The effect of high concentrations of Fe on the elution behavior of the REEs from the LN resin was investigated, leading to the use of AG® MP-1M resin to separate Fe from the REEs in a first phase. Finally, the concentrations of the REEs were determined in permanent magnets and mining concentrates and, for the first time to the best of the authors' knowledge, in metallic samples from a production chain. This project was carried out in the context of the MaDiTraCe[24] project, which aims to enhance transparency, traceability, and sustainability in raw material supply chains.[25]

2. Experimental

2.1. Reagents and materials

High-purity Milli-Q H_2O (>18.2 MΩ cm) was obtained from a Milli-Q Element water purification system (Millipore, France). Pro-analysis 14 M HNO_3 and 12 M HCl (ChemLab, Belgium) were further purified by sub-boiling distillation using a Savillex (USA) DST acid purification system (Savillex Corporation, USA). Ultrapure TraceSELECT® hydrogen peroxide (9.8 M) from Sigma-Aldrich (Belgium) was used without further purification.

The acid digestions were carried out in Teflon Savillex® beakers. For the chromatographic isolations, 2 mL polypropylene columns (8 mm internal diameter) purchased from Eichrom Technologies (USA) were used, along with the corresponding caps, tip closures, and frits. To remove Fe from the digests, columns loaded with 2 mL of AG® MP-1M anion exchange resin (100–200 μm dry mesh size, chloride anionic form, Bio-Rad, Belgium) were used. To separate the REEs from one another, the columns were loaded with 0.78 g of LN resin (100–150 μm dry mesh size), purchased from Eichrom Technologies.

Certified 1.000 g L^{-1} single-element standards for the lanthanides, Y, and ruthenium (Ru) were purchased from Chemlab NV (Belgium), Inorganic Ventures (USA), SCP Science (Canada), and Alfa Aesar – Johnson Matthey (UK). The BHVO-2 reference material was purchased from the United States Geological Survey (USGS, USA).

2.2. Instrumentation and measurements

The determination of REE concentrations was accomplished with an Agilent 7900 quadrupole-based ICP-mass spectrometer

(Agilent Technologies, Japan) equipped with a MicroMist nebulizer and a Peltier-cooled (2 °C) Scott-type spray chamber for sample introduction. The use of this type of standard quadrupole-based ICP-MS instrument was preferred over that of more advanced ICP-MS/MS instrumentation available in the lab to guarantee wide employability of the analytical method developed, as intended in the context of the MaDiTraCe project.

The nuclides ^{89}Y, ^{139}La, ^{140}Ce, ^{141}Pr, ^{146}Nd, ^{147}Sm, ^{153}Eu, ^{155}Gd, ^{159}Tb, ^{163}Dy, ^{165}Ho, ^{166}Er, ^{169}Tm, ^{173}Yb, ^{175}Lu and ^{101}Ru were monitored with an integration time of 1 s. Gd, Tb, Dy, Ho, Er, Tm, Yb and Lu were monitored with the CRC pressurized with He as a collision gas introduced at a flow rate of 4.60 mL min^{-1}, while the rest of the elements were monitored in no gas (CRC vented) mode. Ru, used as an internal standard (IS), was monitored in gas and no-gas mode. Quantification was carried out through external calibration using multi-element calibration standards with a concentration range from 0–0.9 ng mL^{-1}, with 0.3 ng mL^{-1} Ru as an IS. Instrument settings and data acquisition parameters for the Agilent 7900 ICP-MS can be found in Table S1 of the SI. Table S2 summarizes the limits of detection achieved during the quantification of the REEs, calculated as three times the standard deviation of 10 blank measurements divided by the slope of the calibration curve.

2.3. Samples

A summary of the samples included in the study is presented in Table 1.

Fig. S1 illustrates the key steps of the conventional powder metallurgy process used to produce sintered Nd–Fe–B permanent magnets, the most common type on the market. To investigate the impact of (i) strip casting and alloy melting, (ii) hydrogen decrepitation and jet milling, and (iii) compaction, sintering, and machining on the REE distribution pattern, samples provided by the CEA-Liten from four points along a lab-scale production chain were analyzed. The location of the sampling in the production chain is indicated by labels 2–5 in Fig. S1.

All samples were pulverized and analyzed in duplicate. The basalt reference material BHVO-2 (Hawaii) was used to evaluate the accuracy of the results.

2.4. Sample preparation

Fig. 1 presents a schematic diagram of the sample preparation protocol.

One of two digestion procedures was applied depending on the sample type, with around 0.1 g of sample weighed into a pre-cleaned Savillex® Teflon beaker. (1) Concentrate samples underwent an initial digestion with aqua regia (HNO_3 : HCl, 1 : 3) for six days at 90 °C on a heating plate. The solution was then evaporated to dryness at the same temperature, followed by treatment with 8 M HCl for 24 hours. (2) The remaining samples, including the Nd–Pr alloy, ribbons, magnet powder, and magnets, were digested with 8 M HCl on a hot plate at 90 °C for 24 hours. (3) All samples were evaporated to dryness at 90 °C, and all, except those with low Fe concentrations – the Mountain Pass (MP) concentrate and Nd–Pr alloy – were redissolved in 5 mL of 8 M HCl + 0.001% H_2O_2 and submitted to purification (Fe removal) using AG® MP-1M resin. (4) The REEs were separated from Fe using the protocol outlined by Van Heghe *et al.*[26] and Costas-Rodriguez *et al.*[27] for all samples with high Fe concentration – Bayan Obo (BO) concentrate, ribbons, magnet powder, and magnets. Due to the high Fe content in the samples, 2 mL (instead of the usual 1 mL) of analytical grade AG® MP-1M strong anion exchange resin (100–200 μm dry mesh size, chloride anionic form, Bio-Rad, Belgium) were loaded into an Eichrom polypropylene column, subsequently used for chromatographic separation. Prior to use, the resin was cleaned with 10 mL of 7 M HNO_3, followed by 10 mL of MQ water, 10 mL of 0.7 M HNO_3, and 10 mL of MQ water. The resin was then conditioned with 10 mL of 8 M HCl + 0.001% H_2O_2, and the sample was loaded in 5 mL of 8 M HCl + 0.001% H_2O_2. The REEs were collected in the load and matrix wash (3 mL of 8 M HCl + 0.001% H_2O_2). If needed for analysis, the Fe fraction can be collected in 7 mL of 0.53 M HCl. (5) The REE fraction

Table 1 Summary of the samples included in the study

Sample type	Number of samples	Description
(1) REE concentrates	2	Two concentrate samples from two different sources: (i) REE concentrate from Bayan Obo (BO), the world's largest REE mine, which holds vast reserves of Nd, Pr, La, Ce, and Fe, (ii) REE concentrate from Mountain Pass (MP), which was once the world's primary source of REEs and contains high concentrations of Nd and Pr
(2) Nd–Pr alloy	1	A Nd–Pr alloy, used as a raw material. This sample was provided by the French Alternative Energies and Atomic Energy Commission (CEA-Liten)
(3) Ribbons	3	Three samples: two industrial ribbons (Ribbon 1 from Japan, Ribbon 2 from Europe) and one laboratory-made ribbon (Ribbon 3) derived from the same production chain as the Nd–Pr alloy (2), magnet powder (4), and final magnet (5)
(4) Magnet powder	1	Intermediate product obtained from the processing of Ribbon 3. Provided by CEA-Liten
(5) Final magnet	7	Seven sintered Nd–Fe–B magnets: three received from the Geological Survey of Finland (GTK), originating from the same parent magnet; three from the French Geological and Mining Research Bureau (BRGM), also derived from the same wind turbine; and one from CEA-Liten. The latter belongs to the same production chain as the Nd–Pr alloy, Ribbon 3, and magnet powder

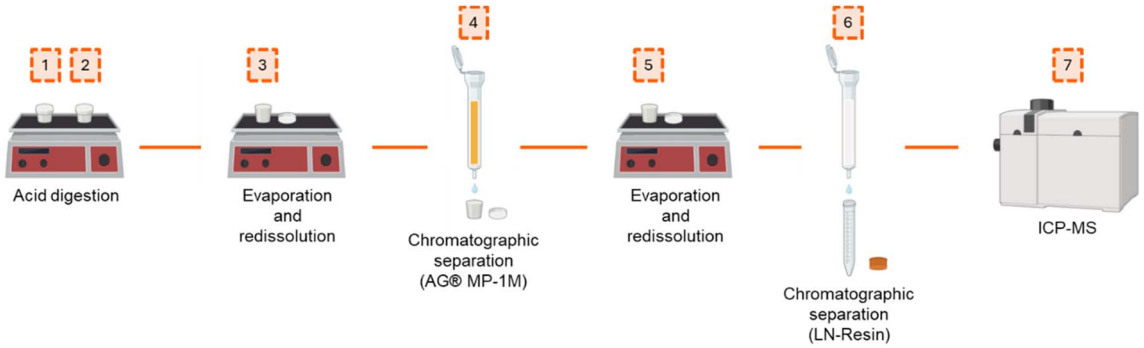

Fig. 1 Schematic overview of the sample preparation protocol.

(sample load + matrix) thus obtained was evaporated to dryness and redissolved in 1 mL of 0.01 M HNO_3. For samples with low Fe content (MP concentrate and Nd–Pr alloy), the dry residue obtained was also redissolved in 1 mL of 0.01 M HNO_3. (6) REE separation was performed according to the protocol described by Arrigo *et al.*[23] Prior to use, 0.78 g of resin was weighed into a 15 mL tube and hydrated with 5 mL of 0.1 M HNO_3 for several hours. The resin was then centrifuged at 3500 rpm for 5 minutes, and the liquid phase was carefully decanted. The resin was loaded into an Eichrom polypropylene column and subsequently cleaned and conditioned with 15 mL of 0.01 M HNO_3. REE separation was accomplished using a progressively increasing concentration of HNO_3 as a mobile phase, as detailed in Table 2.

Eight fractions containing the REEs were collected over a total elution time of 7 hours and subsequently diluted for ICP-MS analysis. To calculate the concentrations of each element, the absolute amount (mass in ng) of each element was determined in each fraction. For elements eluting in more than one fraction, the total amount (mass) was obtained by summing the amounts measured across all relevant fractions.

For samples with $N = 1$, an estimated RSD of 10% was applied, based on the typical variability observed for replicate analyses throughout this study. This value represents a reasonable upper limit for the reproducibility for these sample types.

Table 2 Gradient elution parameters for REE separation using 0.78 g of LN resin with 100–150 μm particle size at a flow rate of 3.33 mL min^{-1}. L, load; M, matrix wash; F, fraction[23]

Fraction	HNO_3 (M)	Volume (mL)	Elements
L0	0.01	20	—
M1	0.05	15	—
M2	0.10	10	—
F1	0.25	10	La, Ce, Pr, Nd, Sm, Eu
F2	0.50	10	Ce, Pr, Nd, Sm, Eu, Gd
F3	0.75	10	Gd, Tb
F4	1.0	10	Tb, Dy, Ho
F5	1.5	4	Dy, Ho
F6	2.0	4	Y, Dy, Ho, Er
F7	2.5	4	Y, Ho, Er
F8	8.0	30	Y, Ho, Er, Tm, Yb, Lu

A procedural blank and the reference material BHVO-2 were treated in the same manner for each batch of samples.

2.5. Mathematical correction for oxide and hydroxide interferences

Mathematical correction was evaluated for addressing the interference caused by oxide and hydroxide ions in the determination of REEs in permanent magnets. This approach relied on quantification of the formation levels of $REEO^+$ and $REEOH^+$ species while monitoring 1 μg L^{-1} mono-elemental REE standard solutions. Based on the intensities measured at the m/z values corresponding to the nuclides monitored for the HREE, correction factors were calculated based on the ratio of the oxide or hydroxide ion signal to the corresponding M^+ signal for the parent nuclide:

$$f_{REEO^+} = \frac{I_{REEO^+}}{I_{REE^+}} \quad (1)$$

The factors thus obtained were subsequently applied to estimate/calculate the contribution of the oxide or hydroxide ion interferences to the signals measured for the affected HREEs in the multi-element solutions and subtract these from the corresponding total signal intensities (2):

$$I_{corrected} = I_{measured} - f_{REEO^+} \cdot I_{REE^+} \quad (2)$$

where $I_{corrected}$ is the true signal for the analyte, $I_{measured}$ is the raw intensity at the affected m/z, f_{REEO} is the experimentally determined correction factor, and I_{REE} is the intensity of the interfering REE parent nuclide.

3. Results and discussion

3.1. Evaluation of mathematical correction for interference by oxide and hydroxide ions

In Nd–Fe–B permanent magnets, the concentration of some LREEs is significantly higher than that of HREEs. This "imbalance" leads to LREE oxide and hydroxide ions potentially having a substantial effect on the concentration values obtained for the HREEs if not avoided or properly corrected for. Accurate quantification requires addressing these interferences either

mathematically or through physical (chromatographic) separation of the elements prior to analysis.

Table S3 lists the isotopes of the elements of interest, their isobars, and the interfering LREE oxide and hydroxide ions. Given that Nd typically represents between 20% and 30% of the total mass in these magnets,[28] its oxide and hydroxide species are particularly problematic, jeopardizing the accurate determination of several HREEs, notably Tb, Dy, Ho, and Er. As such, Nd constitutes the most critical interfering element in this matrix, and it is necessary to evaluate whether mathematical correction is sufficient to ensure accurate results.

To this end, a set of mixtures containing fixed concentrations of Tb, Dy, Ho, and Er were prepared with increasing levels of Nd, yielding concentration ratios (HREE : Nd) of 1 : 10, 1 : 20, 1 : 50, 1 : 500, and 1 : 1500. Fig. 2 shows the recoveries for the selected HREEs (Tb, Dy, Ho, and Er) for the 1 : 50, 1 : 500, and 1 : 1500 HREE : Nd ratios, both before and after mathematical correction.

The 1 : 10 and 1 : 20 ratios were not included, as no significant differences were observed between the corrected and uncorrected values, with recoveries ranging between 90% and 110% in all cases. For the 1 : 50 ratio, all corrected and uncorrected values fall within the 90–110% range, except for that for Dy, which shows a recovery of 117.5 ± 0.4% without correction and 103.1 ± 0.6% after correction. As the concentration difference between Nd and the HREEs increases, the contribution of Nd oxide and hydroxide ions becomes more pronounced, resulting in Dy recoveries reaching up to 442.0 ± 7.2% at an HREE : Nd ratio of 1 : 1500. At a 1 : 500 ratio, the mathematical correction still proved effective for all elements except for Er, for which the recovery was still >110% (114.2 ± 2.5%) after correction. Surprisingly, at the 1 : 1500 ratio, correction was successful for both Er (101.4 ± 1.1%) and Ho (96.4 ± 2.1%), which is consistent with the fact that Ho is the least affected by Nd-based interferences among the four elements. In contrast, the correction failed for Tb and Dy, yielding recoveries of 69.9 ± 1.6 and 5.6 ± 2.9%, respectively.

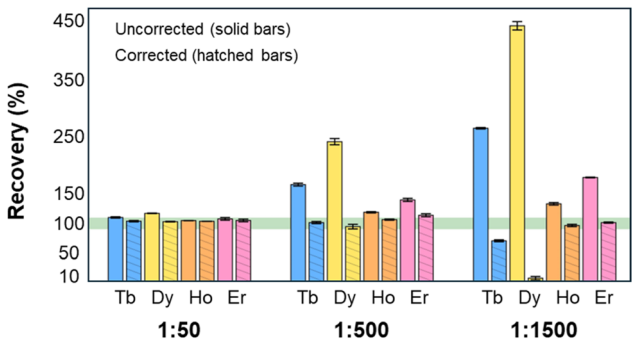

Fig. 2 Recoveries for Tb, Dy, Ho, and Er for standard solutions with 1 : 50, 1 : 500, and 1 : 1500 HREE : Nd ratios, both before and after mathematical correction. The solid bars represent the uncorrected recoveries, while the hatched bars represent the corrected recoveries. Error bars represent intermediate error, expressed as SD from $N = 3$ replicates. The green line represents the accepted recovery range of 90% to 110%.

In Nd-based permanent magnets, the concentration ratio between Nd and HREEs can exceed 1 : 1500. Under such extreme conditions, mathematical correction of polyatomic interferences becomes unreliable. Moreover, implementing this approach requires concurrent measurement of the intensities for both the Nd parent nuclide at the origin of the interference and the HREE nuclide affected. This leads to Nd signal intensities often exceeding one million counts per second, triggering the instrument's detection system to switch from pulse counting to analog mode. This transition can compromise the quantification accuracy unless there is very careful cross-calibration between the two modes. As a result, the mathematical correction becomes less effective and, in some cases, invalid results are obtained. Therefore, the only viable alternative is to physically separate the interfering elements and the elements interfered with in order to obtain reliable results.

3.2. Evaluation of the HNO_3 gradient for REE separation

For the analysis of permanent magnets and production chain samples, complete separation of all the lanthanides from one another is not required, as long as the REEs forming polyatomic interferences are effectively separated from those affected by these interferences. The elution gradient optimized by Arrigo *et al.*[23] for 1.56 g LN resin (100–150 μm) was evaluated using half the amount of resin in order to reduce separation times (for details about the LN resin mass, see the SI), while assessing the efficiency of the separation.

A mass of 0.78 g LN resin (100–150 μm) and a multi-element REE mixture, representing the composition of a Nd–Fe–B permanent magnet based on the values reported by X. Liu *et al.*,[29] were used. The concentration values used for the simulation of the magnet composition are provided in Table 3.

Iron was deliberately excluded from the mixture in this experiment because the resin specifications indicate that the elution behavior is affected by high Fe concentrations.[30]

Fig. 3(A–C) compiles graphs showing the concentrations for REEs affected by polyatomic interferences, as well as those generating these interferences, across the different fractions (F1–F8).

Table 4 presents the recovery values for all the elements in the multi-element mixture.

The two Gd isotopes free from isobaric interferences, ^{155}Gd and ^{157}Gd, are predominantly affected by polyatomic interferences from LaO^+ (^{155}Gd) and from $CeOH^+$ and PrO^+ (^{157}Gd), respectively. In graph A of Fig. 3, it can be observed that La and Ce (both referenced to the right axis) elute entirely in the first fraction (F1), whereas the majority of the Pr elutes in the first fraction and partially in the second (F2), at a concentration similar to that of Gd in this second fraction. By using the ^{155}Gd isotope, accurate quantification can be achieved. The recovery for Gd was 97.8 ± 4.1%, while Pr, La and Ce showed recoveries of 101.6 ± 3.9%, 100.0 ± 2.3% and 103.0 ± 2.5, respectively.

As shown in Fig. 3B, Yb, Tm, and Lu elute entirely in fraction F8, with recoveries of 120.3 ± 5.8%, 110.6 ± 4.2%, and 107.3 ± 7.1%, respectively. The most abundant isotopes of Yb (^{171}Yb, ^{172}Yb, and ^{173}Yb) are mostly interfered with by the oxide and

Table 3 Multi-element REE mixture representing a permanent magnet based on the values reported by X. Liu *et al.*[29]

		Multi-element solution (μg L^{-1})
Elements present at the percentage (%) level in magnets	Fe	650
	Nd	250
Major components (>1000 μg kg^{-1})	Pr	40
	Gd	1
	Dy	30
Minor components (>10 μg kg^{-1} but ≤1000 μg kg^{-1})	La, Ce, Y, Sm, Tb, Ho, Er	0.10
Trace amounts (<10 μg kg^{-1})	Eu, Tm, Yb, Lu	0.01

hydroxide ions of the different isotopes of Gd, which elutes prior to F3. Tm is a mono-isotopic element (^{169}Tm) and is primarily affected by the oxide ion of Eu, which, similarly to Gd, elutes prior to F3 (104.2 ± 6.2% recovery). Additionally, the signal of ^{169}Tm may also be affected by that of hydroxide ions of ^{152}Gd (which displays a very low natural abundance) and ^{152}Sm, with Sm typically present at low concentrations in the samples. Moreover, Sm eluted in F1 and F2 (110.4 ± 3.5% recovery), so it would not interfere with the quantification of Tm. Finally, ^{175}Lu is mainly affected by the oxide of Tb, which, as shown in Fig. 3B and C, elutes before F4. The elevated recovery of Yb, as well as the slightly elevated recoveries of Tm and Lu, can likely be attributed to the high acid concentration (8 M HNO_3) in F8, which may cause a minor matrix-induced enhancement of the ICP-MS signal.

As previously mentioned, Nd is present in permanent magnets at a level of 20% to 30%, and its oxides and hydroxide ions critically interfere with the quantification of Tb, Dy, Ho, and Er. As shown in Fig. 3C, Nd (refer to the left *Y*-axis) elutes in the first two fractions (100.7 ± 4.9% recovery), while the four elements affected begin to elute from the third fraction onwards only. Tb is a mono-isotopic element that, in addition to being affected by the occurrence of NdO^+ and $NdOH^+$, may also be interfered with by that of $CeOH^+$. However, as shown in Fig. 3A, Ce elutes entirely in F1 and therefore $CeOH^+$ does not affect Tb quantification (101.3 ± 5.4% recovery). The two Dy isotopes free from isobaric interference, ^{161}Dy and ^{163}Dy, can also be affected

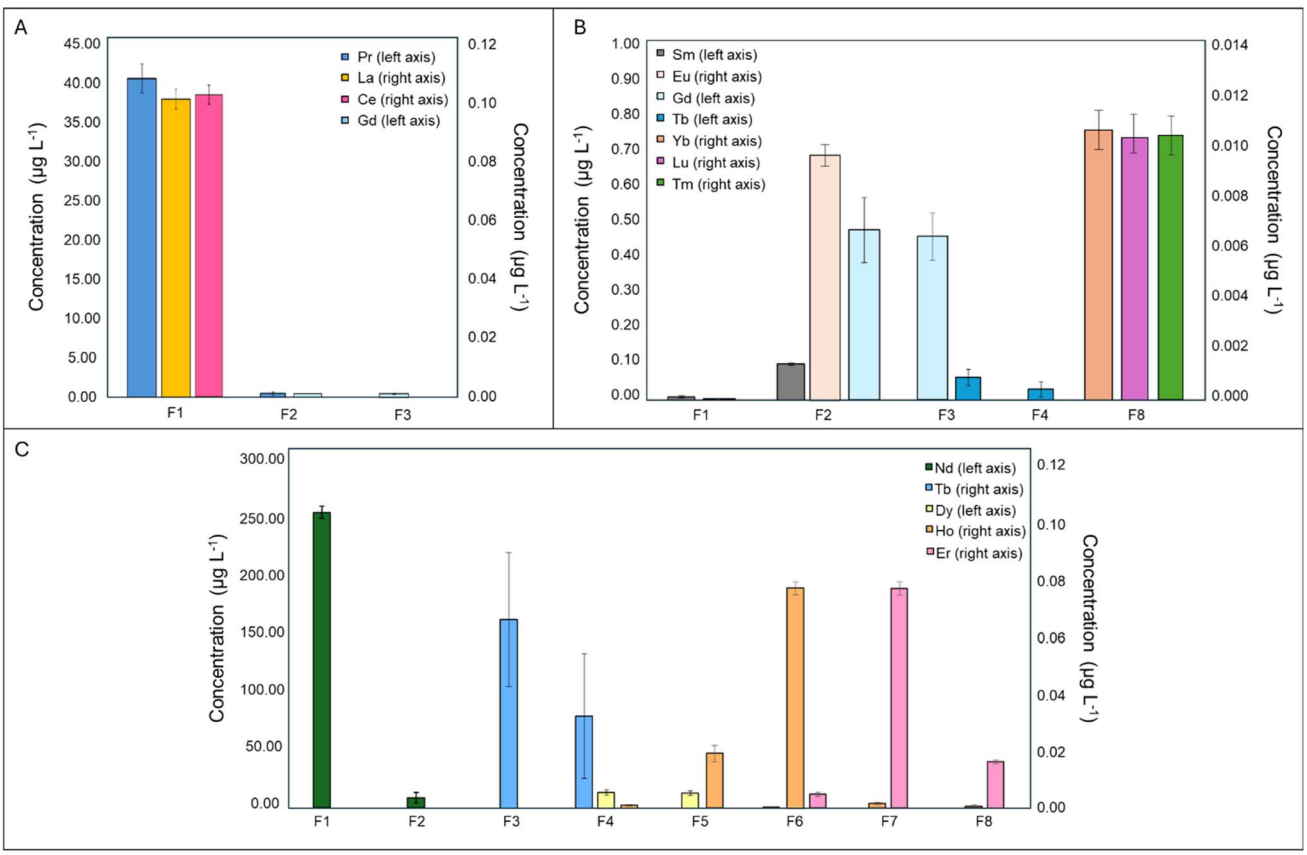

Fig. 3 Distribution of element concentrations (μg L^{-1}) across the different chromatographic fractions (F1–F8) for a multi-element REE mixture, representing the composition of a Nd–Fe–B permanent magnet. Error bars represent intermediate error, expressed as SD from $N = 3$ replicates. (A) Pr and Gd are plotted against the left *Y*-axis, while La and Ce are plotted against the right *Y*-axis. (B) Sm, Gd and Tb are plotted against the left *Y*-axis, and Eu, Yb, Lu and Tm against the right *Y*-axis. (C) Nd and Dy are plotted against the left *Y*-axis, and Tb, Ho and Er against the right *Y*-axis.

Table 4 Recovery values for a multi-element mixture of REEs representing a Nd–Fe–B permanent magnet[29] in the presence and absence of Fe. Standard deviation calculated from $N = 9$ replicates in the absence of Fe and $N = 6$ in the presence of Fe

E	Recovery (%)	Recovery in the presence of Fe (%)	E	Recovery (%)	Recovery in the presence of Fe (%)
Y	102.4 ± 5.1	99.4 ± 7.1	Tb	101.3 ± 5.4	130.8 ± 18.4
La	100.0 ± 2.3	97.7 ± 2.7	Dy	93.8 ± 1.9	102.4 ± 8.6
Ce	103.0 ± 2.5	101.2 ± 2.8	Ho	100.7 ± 3.6	111.5 ± 5.0
Pr	101.6 ± 3.9	103.7 ± 4.3	Er	100.0 ± 3.8	107.7 ± 4.8
Nd	100.7 ± 4.9	103.0 ± 2.2	Tm	110.6 ± 4.2	114.1 ± 5.3
Sm	110.4 ± 3.5	81.5 ± 1.9	Yb	120.3 ± 5.8	123.0 ± 3.3
Eu	104.2 ± 6.2	98.1 ± 2.3	Lu	107.3 ± 7.1	118.5 ± 2.9
Gd	97.8 ± 4.1	110.6 ± 3.5			

by Sm-derived polyatomic interferences, in addition to those from Nd. Ho behaves similarly, as its only isotope (^{165}Ho) is also affected by SmO^+ and $SmOH^+$ interferences. However, as previously mentioned, Sm is typically present at low concentrations in the samples and is distributed over fractions 1 and 2 (Fig. 3B), minimizing its impact on Dy and Ho. The recoveries for Dy and Ho were 93.8 ± 1.9% and 100.7 ± 3.6%, respectively. The Er isotopes free from isobaric interference are ^{166}Er and ^{167}Er. In addition to interferences from Nd and Sm oxide and hydroxide ions, ^{167}Er may also be affected by EuO^+. However, like Sm, Eu is typically present at low concentrations in Nd-based permanent magnets. As shown in Fig. 3B, Eu elutes in F1 and F2 and therefore does not significantly interfere with Er quantification, as Er begins to elute from F6 onwards (100.0 ± 3.8% recovery).

By applying the previously optimized elution gradient,[23] REEs affected by polyatomic interferences were effectively separated from the elements at the origin of these interferences, as most of the REEs otherwise affected elute in the later fractions. Recoveries for all elements (Table 4), except for Yb, remained within or at least close to the acceptable range of 90–110%, with slight deviations observed for Sm (110.4%) and Tm (110.6%). Only Yb showed a notably higher recovery (120.3 ± 5.8) attributed to a minor matrix-induced enhancement of the ICP-MS signal due to the high acid concentration in fraction F8. Overall, the results confirm the suitability of the elution conditions for the separation of REEs present in Nd-based permanent magnet matrices, thus allowing their reliable subsequent determination using quadrupole-based ICP-MS.

3.3. Evaluation of the effect of a high Fe concentration on the LN resin

As previously mentioned, the elution of the REEs from LN resin is affected by a high Fe concentration.[30] Permanent Nd–Fe–B magnets typically contain more than 65% Fe. To investigate the effect of Fe on the LN resin, a resin mass of 0.78 g was used, and a multi-element REE mixture representative of a permanent magnet (Table 3) was loaded onto the column.

The elution of LREEs was significantly altered compared to the behavior observed under optimal conditions. As an example, Fig. 4 illustrates the distribution of the concentrations of Nd (Fig. 4A) and Pr (Fig. 4B), the two most abundant REEs in permanent magnets, in the various fractions under both conditions, *i.e.* in the presence and absence of Fe.

In the absence of Fe in the multi-element REE mixture, both elements eluted within the first two fractions. However, when Fe was present, their concentrations were distributed across all fractions collected. The recovery in the presence of Fe for both elements was complete when summing the amounts (masses) distributed across all fractions (103.0 ± 2.2% for Nd and 103.7 ± 4.3% for Pr). Recovery values for all elements in the multi-element mixture with Fe are also provided in Table 4.

Similar behavior was observed for the other LREEs (La, Ce, Sm and Eu), indicating that high Fe concentrations can affect the selectivity of the LN resin toward LREEs, thereby altering their elution profiles. No significant differences were observed in the recoveries of La, Ce, and Eu in the presence or absence of Fe. In contrast, a marked decrease in Sm recovery was detected

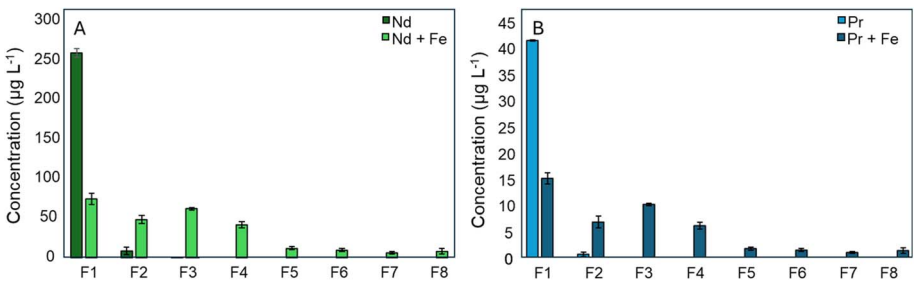

Fig. 4 Distribution of Nd (A) and Pr (B) concentrations (µg L^{-1}) across the different fractions (F1–F8) with and without Fe in the multi-element REE mixture, the composition of which represents a permanent magnet. Error bars represent intermediate error, expressed as SD from $N = 3$ replicates.

in the presence of Fe, possibly due to a shift of Sm toward the lower molarity fractions (81.5 ± 1.9%).

The elution behavior of Gd and Dy was also affected by the presence of Fe, resulting in a broadening of their elution profiles. As previously mentioned, Gd quantification can be performed using both ^{155}Gd (mainly interfered with by LaO^+) and ^{157}Gd (interfered with by PrO^+ and $CeOH^+$). The altered elution of Pr and Ce in the presence of Fe, combined with the high concentration of Pr in the multi-element mixture, resulted in inaccurate quantification based on ^{157}Gd, with recovery values reaching as high as 191.9%. However, considering that La is present at a lower concentration than Gd, more accurate quantification was possible when using ^{155}Gd, yielding a recovery of 110.6 ± 3.5% in the presence of Fe despite the co-elution of Gd and La. For Dy, ^{163}Dy (interference from $NdOH^+$ and SmO^+) was used. Because Dy is present at much higher concentrations than Sm in the multi-element mixture and the Nd-to-Dy ratio does not exceed 1 : 10, quantification was not affected by their co-elution. As a result, Dy recovery in the presence of Fe was 102.4 ± 8.6%.

High Fe concentrations also compromise the accurate quantification of Tb. The determination of Tb is subject to interference from NdO^+, $NdOH^+$ and $CeOH^+$, and due to the altered elution behavior of Nd and Ce, oxide and hydroxide ion formation leads to an overestimation of the Tb concentration. Assuming that the elution profile of Tb is not broadened by Fe and that it remains fully eluted within the same fractions as in the absence of Fe (F3 and F4), the calculated recovery of Tb is 130.8 ± 18.4%.

Elution profiles of elements eluting at lower pH values do not exhibit any noticeable broadening. Specifically, no significant differences were observed in the recoveries of Tm and Y in the presence or absence of Fe. Yb recoveries also remained consistent across both conditions, although they were relatively high overall (120.3 ± 5.8% in the presence of Fe). In contrast, the recoveries for Ho, Er, and Lu were slightly higher in the presence of Fe (111.5 ± 5.0%, 107.7 ± 4.8% and 118.5 ± 2.9%, respectively). For Ho and Er, this effect can be attributed to the formation of Nd hydroxide ions in the plasma. The higher recovery for Lu could tentatively be explained by an effect on the elution profile of Tb. For the calculation of the recovery of Tb, it was assumed that the element elutes in F3 and F4, but in fact it is impossible to distinguish the Tb signal from that of NdO^+ and $NdOH^+$.

Given the impact of Fe on the elution and quantification of LREEs Gd, Dy, and especially Tb, the separation of Fe from the REEs was considered essential to ensure accurate quantitative determination.

3.4. Evaluation of the AG® MP-1M resin for the separation of Fe and REEs

Several methods have been proposed for the separation of Fe from the REEs in iron-rich samples, including precipitation. However, this approach has associated issues; it is not only time-consuming, but also the potential coprecipitation of Ln^{3+} ions needs to be considered.[31] Most authors have employed chromatographic techniques using cationic resins, such as 50WX4 strong acid cation exchange column[32] or AIR120H resin.[33]

In this work, the AG® MP-1M strong anion exchange resin was used following the procedure developed by Costas-Rodriguez *et al.*[27] This resin allows the isolation of Fe and Cu, as Fe^{3+} and Cu^{2+} form anionic complexes in the presence of chlorides, unlike Ln^{3+} ions, which are not retained.

To assess the separation of Fe and REEs using AG® MP-1M resin, a mixture of 50 μg of the lanthanides and 50 μg of Fe was loaded onto 1 mL of AG® MP-1M resin. Since the REEs were not retained by the anion exchange resin, they were completely eluted within the sample load and the matrix fractions, with recoveries ranging from 98% to 106% (Table S4). Fe was also quantitatively recovered, with recoveries between 98% and 101%. To ensure complete removal of Fe from real samples, given the high iron content in permanent magnets, 2 mL of resin were loaded into the columns instead of the standard 1 mL.

3.5. QA/QC measurements

Quality assurance and quality control of the measurements was performed during each analytical session by processing the certified reference material BHVO-2 (a basaltic rock standard from Hawaii containing 8.63 ± 0.14 wt% of Fe)[34] using the same separation procedure applied to the samples, based on the use of both AG® MP-1M and LN resin (100–150 μm). While BHVO-2 does not replicate the metallic matrix of Nd–Fe–B alloys, its basaltic composition represents a challenging matrix that complements the REE concentrates studied. Additionally, a procedural blank was included in each measurement session.

Interference removal was confirmed using multi-element spike experiments, with recoveries ranging from 90 to 110% for the majority of REEs, demonstrating the reliability of the method (see Sections 3.2. and 3.3). In addition, for elements such as Ce, Nd, and Pr, which elute across multiple chromatographic fractions in the presence of Fe, the sum of the relevant fractions is in good agreement with bulk measurements, confirming effective Fe removal and accurate quantification (Table S5).

The experimental values obtained for the BHVO-2, along with the certified values and procedural blank results, are presented in Table 5. The values for the reference material were corrected by subtracting the contribution from the procedural blank, calculated based on a theoretical sample mass of 0.1 g.

Most of the experimental values obtained for the reference material are consistent with the certified values, falling within the ± 2 standard deviation interval (La, Ce, Sm, Eu, Dy, Er, Tm, and Lu). The results for some elements, such as Gd and Ho, show minor discrepancies but the results are still very close to the certified range. On the other hand, the results for elements like Y, Nd, Pr, Tb, and Yb lie outside the expected interval.

In the case of Nd and Pr, the low recovery can be attributed to high procedural blanks (see Table 5). However, this does not affect the measurement of these elements in the real samples, as both Nd and Pr are present at the ten percent level. Therefore, contamination at the μg g^{-1} level has no significant impact on

Table 5 Reference and experimental values for BHVO-2 reference material,[34] along with procedural blanks, obtained in each measurement session. The procedural blank value was calculated based on a theoretical sample mass of 0.1 g. Uncertainty expressed as ± SD. <LoQ indicates values below the quantification limit

E	Reference values (μg g^{-1})	Experimental values (μg g^{-1})	Procedural blank (μg g^{-1})
Y	25.91 ± 0.28	22.2 ± 1.1	0.09
La	15.20 ± 0.08	14.94 ± 0.88	0.7
Ce	37.53 ± 0.19	35.3 ± 1.5	1.3
Nd	24.27 ± 0.25	22.53 ± 0.040	3
Pr	5.339 ± 0.028	4.88 ± 0.17	0.7
Sm	6.023 ± 0.057	5.11 ± 0.51	0.05
Eu	2.043 ± 0.012	1.93 ± 0.13	0.02
Gd	6.207 ± 0.038	5.80 ± 0.18	0.06
Tb	0.9392 ± 0.0060	0.848 ± 0.026	0.005
Dy	5.280 ± 0.028	4.92 ± 0.24	0.06
Ho	0.9887 ± 0.0053	0.906 ± 0.029	0.006
Er	2.511 ± 0.014	2.40 ± 0.14	0.006
Tm	0.3349 ± 0.0031	0.3094 ± 0.0083	0.002
Yb	1.994 ± 0.027	1.792 ± 0.059	0.007
Lu	0.2754 ± 0.0024	0.258 ± 0.025	<LoQ

their accurate determination. Moreover, both elements can be reliably quantified through bulk analysis (without Fe removal and REE separation). The low recovery observed for Y may be attributed to strong retention on the resin, hindering complete elution, despite full recovery being observed for the multi-element mixture. As with Nd and Pr, Y can also be quantified in the bulk solution. In the case of Tb, partial elution in F2, alongside Nd, could explain the incomplete recovery. For Yb, however, no clear explanation is available. While its recovery in the multi-element mixture exceeded 110%, in this case it dropped below 90% (89.87%), without obvious analytical cause.

Most procedural blanks are in the ng g^{-1} range, with values for Tb, Ho, Er, Tm, and Yb below 10 ng g^{-1}, and those for Y, Sm, Eu, Gd, and Dy below 100 ng g^{-1}. The procedural blank for Lu was below the detection limit. In contrast, the blanks for the most abundant elements in the samples were significantly higher: blank values for La, Ce, and Pr were around 1 μg g^{-1}, and the value for Nd reached approximately 3 μg g^{-1}. These higher blank values are attributed to sample contamination, most likely originating from the previous digestion of highly concentrated samples in the same Teflon beakers. The beakers were cleaned following a four-step protocol consisting of two treatments with 50% HNO_3 and two treatments with 50% HCl on a hot plate at 110 °C. However, given the very high REE concentrations of the samples analyzed in this study, it is possible that trace level carryover occurred. When subsequently processing BHVO-2, which contains significantly lower concentrations of Nd, Pr, La, and Ce compared to the samples, this cleaning protocol may not have been sufficient to completely eliminate residual contamination.

3.6. Sample results

The values obtained for the entire set of samples analyzed are presented in Fig. 5A–D, after chondrite normalization[35] and logarithmic scaling. Because interpretation of chondrite-normalized patterns can be less intuitive from a process-engineering perspective, we additionally report and discuss REE abundances relative to the total REE content ($REE_i/\Sigma REE$) for each sample (SI Tables S6 and S7).

3.6.1. Bayan Obo and Mountain Pass concentrates. Fig. 5A illustrates the chondrite-normalized REE patterns for the Bayan Obo and Mountain Pass concentrates analyzed (on a logarithmic scale). Both Bayan Obo and Mountain Pass rank among the world's largest REE sources and are characterized by a pronounced enrichment in LREEs compared to HREEs. This characteristic is clearly reflected in the decreasing trend observed from LREEs to HREEs in the graph presented in Fig. 5A, which is consistent with observations reported in the literature.[36,37]

In both concentrates, all LREEs occur at percentage levels relative to the total REE budget ($REE_i/\Sigma REE$), with La and Ce being by far the most abundant, whereas Eu remains at sub-percent levels. La and Ce together account for ≈80% of the ΣREE in the Mountain Pass concentrate (La = 33.7%, Ce = 48.7%) and ≈76% in the Bayan Obo concentrate (La = 27.1%, Ce = 49.0%). In contrast, Nd and Pr represent a smaller fraction of the ΣREE in the concentrates (Nd = 12.2–16.7%, Pr = 4.2–5.0%), whereas Nd and Pr dominate the REE budget in Nd–Fe–B permanent magnets.

All HREEs are found at concentrations in the μg g^{-1} range. Lu displays the lowest HREE concentrations, with values of 1.24 μg g^{-1} in the Mountain Pass concentrate and 0.59 μg g^{-1} in the Bayan Obo concentrate. The patterns of both concentrates are very similar for the LREEs, whereas for the HREEs, Bayan Obo is more enriched than Mountain Pass, with the exception of Tm, Yb and Lu. The total REE contents of these concentrates are on the order of ≈50 wt%, substantially higher than in downstream Nd–Fe–B alloys and magnets (≈30 wt%), reflecting dilution by Fe and other alloying elements along the value chain.

These types of concentrates typically serve as raw materials for the production of magnets, undergoing significant transformations from the concentrate stage to the alloy stage (*i.e.* Nd–Pr alloy). This is reflected in the differences between the

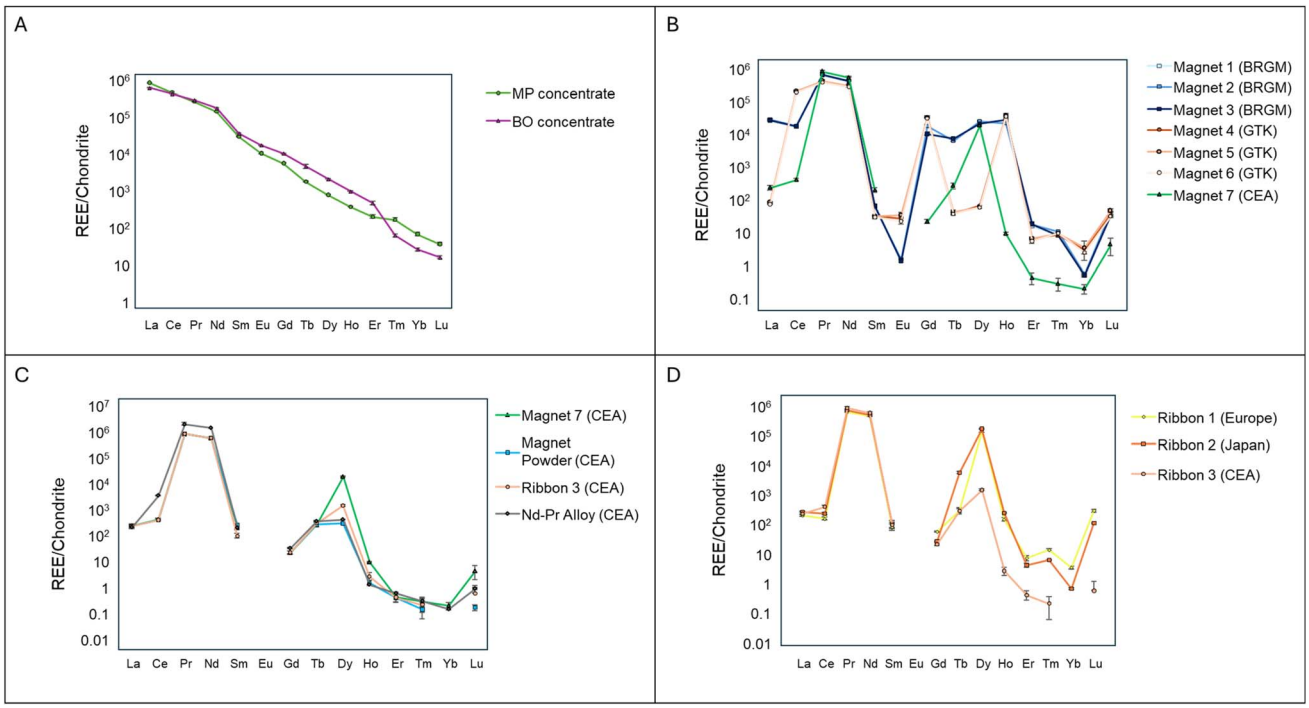

Fig. 5 Chondrite-normalized REE patterns for: (A) Mountain Pass (MP) and Bayan Obo (BO) concentrates, (B) magnets received from BRGM, GTK, and CEA-Liten, (C) samples from the value chain provided by CEA-Liten, and (D) ribbons. The *Y*-axis is on a logarithmic scale. Error bars represent the SD. The number of replicates per point ranged from $N = 1$ to 4. For samples with $N = 1$, a relative standard deviation (RSD) of 10% was used as an SD estimate.

patterns of the concentrates (Fig. 5A) and those of the subsequent samples (Fig. 5B–D) from the magnet production chain. In this context, elemental REE patterns alone are not sufficient to demonstrate whether specific concentrates were used to produce a given downstream material. Accurate determination of whether the concentrates used in the production of a given sample originate from the Bayan Obo mine, Mountain Pass, or any other deposit worldwide requires comprehensive knowledge of the chemical and isotopic characteristics of REE deposits. While REE patterns combined with major and trace element compositions already provide valuable information, more advanced approaches, such as isotopic analysis, appear particularly relevant for robust source attribution. In this respect, measuring Nd isotope ratios represents a promising avenue, given their documented variability among geological sources.[38]

3.6.2. Nd–Fe–B permanent magnets. Fig. 5B presents the chondrite-normalized REE patterns of the seven magnets analyzed, revealing three distinct trends. Despite some analytical noise, all patterns exhibit an overall decreasing trend from LREEs to HREEs, with prominent enrichments in Nd and Pr, consistent with the composition of Nd–Fe–B permanent magnets.

Data for the three magnets, provided by BRGM, are plotted in blue as square symbols in Fig. 5B and show identical REE values, except for one replicate, which displays slightly elevated Gd and Ho concentrations. In terms of REE abundances relative to the total REE budget (REE□/ΣREE), Nd and Pr together account for ≈90% of the ΣREE (Nd ≈ 70–71%, Pr ≈ 20%, Table S6), whereas La and Ce contribute ≈2–4% only (La ≈ 2.1–2.2%, Ce = 3.7%). Gd, Dy and Ho occur at the percent level (Gd ≈ 0.7–1.3%, Dy ≈ 1.8–2.1%, Ho ≈ 0.39–0.53% of the ΣREE; Table S7), in line with deliberate Dy and Gd additions to enhance coercivity. The three BRGM samples (coming from a single wind turbine) are compositionally very similar and likely originate from the same production batch, with only minor differences for a few HREEs (Gd, Ho, Dy, Tb).

Similarly, the three magnet samples received from GTK (data in orange, circles in Fig. 5B) come from the same parent magnet and yield identical values across all the REEs. Bulk Nd and Pr concentrations are lower than in the BRGM magnets (see Table S6), while the Ce concentration is substantially higher. When expressed as $REE_i/\Sigma REE$, Ce represents ≈39% of the total REEs (38.8–39.1%), compared with only ≈3.7% in the BRGM magnets, whereas Nd and Pr account for ≈46% and ≈12%, respectively. La contributes to a few percent, and Gd and Ho occur at the percent level (Gd ≈ 2.1–2.3%, Ho ≈ 0.61–0.65% of the ΣREE). Dy and Tb, in contrast, are present at much lower levels than in the BRGM magnets and no significant Dy- or Tb-enrichment is observed. Overall, the GTK magnets correspond to a Ce-rich Nd–Fe–B composition with very limited addition of heavy REEs.

Results for the magnet sample from CEA-Liten are shown in green in Fig. 5B. This sample is compositionally distinct from both the BRGM and GTK magnets. It was manufactured from an Nd–Pr alloy specifically designed to contain Nd and Pr only (*i.e.* without Ce, La or HREEs), and this is reflected in the very high Nd and Pr fractions relative to the ΣREE (Nd ≈ 77%, Pr ≈ 21%)

and the very low Ce and La contents (in the order of a few hundred μg g^{-1} in the bulk). Eu remains below the procedural blank for the CEA magnet, and its Gd content is significantly lower (≈10–15 μg g^{-1}) than in the BRGM and GTK magnets, where Gd occurs at the percent level relative to the ΣREE. For HREEs, Dy occurs at percent-level concentrations in both the BRGM and CEA-Liten magnets (Dy ≈ 1.3–2.1% of ΣREE), whereas in the GTK magnets the occurrence of Dy is restricted to the μg g^{-1} range. Ho is present at percent-level concentrations in the BRGM and GTK magnets but is strongly depleted in the CEA-Liten magnet, where it only reaches ≈1–2 μg g^{-1}. Er, Tm, Yb and Lu occur at sub- to low-μg g^{-1} levels in all magnets; in the CEA-Liten magnet, Er, Yb and Lu remain below ≈0.3 μg g^{-1}, while the Tm concentration is around 0.02 μg g^{-1}. Y concentrations are similar in the BRGM and GTK magnets, whereas the CEA-Liten magnet shows clearly lower Y contents.

Overall, these patterns reflect the intentional enrichment of specific REEs during Nd–Fe–B magnet production, as well as differences in supplier feedstocks and alloying strategies. In particular, the Ce-rich GTK magnets illustrate the use of Ce as a partial substitute for Nd and Pr, whereas the BRGM and CEA-Liten magnets rely more strongly on Nd–Pr-rich compositions with variable additions of Dy, Gd and Ho to tailor coercivity.

3.6.3. Value chain samples. As explained in the 'Samples' section, different samples from the production chain (Fig. S1) were selected to study the effects of (i) strip casting and alloy melting, (ii) hydrogen decrepitation and jet milling, and (iii) compaction, sintering and machining on the REE distribution patterns. Fig. 5C displays the chondrite-normalized REE patterns (on a logarithmic scale) for the Nd–Pr alloy, strip-cast ribbon, magnet powder and final magnet, all originating from the same production chain and provided by CEA-Liten.

From Fig. 5C, it is evident that the REE patterns across the different stages of the production chain exhibit a very consistent distribution, characterized by a general decreasing trend from LREEs to HREEs. Eu concentrations are not displayed, as they remained below the procedural blank level in all samples. Similar to the Nd–Fe–B magnets, the value-chain samples show a pronounced enrichment in Nd and Pr. In terms of $REE_i/\Sigma REE$, Nd and Pr together account for approximately 98–100% of ΣREE in the Nd–Pr alloy, ribbon, magnet powder and final magnet (Nd ≈ 77–79%, Pr ≈ 20–22%; Table S6), whereas La, Ce and the HREEs together contribute only a few percent of the total REE budget.

The Nd–Pr alloy was designed to have a simple Nd–Pr-only composition. Nevertheless, minor amounts of other REEs are detected. Along the production chain, small but systematic changes are observed for some of these trace REEs. Ce, for example, is present at ≈330 μg g^{-1} (relative to the ΣREE) in the alloy and this value increases by approximately a factor of two in the ribbon, magnet powder and final magnet (Ce ≈ 650–700 μg g^{-1}; Table S6). Gd shows a similar increase, from ≈7–8 μg g^{-1} in the alloy to ≈12 μg g^{-1} in the ribbon, powder and magnet. These trends are consistent with minor interaction between the molten alloy and the alumina crucible and/or slight carry-over from previous strip casting of Ce-containing (and, to a lesser extent, Gd-containing) material in the same crucible, as observed in CEA-Liten production trials. However, the data available do not allow an unambiguous attribution of the Ce increase to a single mechanism.

Sm concentrations normalized to the ΣREE are lowest in the alloy and ribbon (Sm ≈ 36–42 μg g^{-1}) and distinctly higher in the magnet powder and final magnet (Sm ≈ 90–110 μg g^{-1}; Table S6). This behavior agrees with the industrial observation that jet-milling equipment can retain the material from earlier use; in this case, previous processing of Sm–Co alloys in the same mill may explain the Sm enrichment in the powder and its transfer into the final magnet. Y remains close to 4–5 μg g^{-1} in all four samples, indicating that the overall Y budget is not substantially modified along the chain.

For the HREEs, Tb and Dy display the most noticeable variations. In the Nd–Pr alloy, Tb and Dy occur at modest levels (Tb ≈ 14 μg g^{-1}, Dy ≈ 110 μg g^{-1}; Table S7). Dy becomes markedly enriched in the ribbon (≈950 μg g^{-1}) and remains higher than in the alloy in both the magnet powder (≈200 μg g^{-1}) and the final magnet, where Dy reaches percent-level abundances relative to ΣREE (Dy ≈ 1.3%). This progression is consistent with Dy contamination from previous Dy-bearing alloys processed in the same equipment during strip casting and sintering. Ho, Er, Tm, Yb and Lu remain at sub- to low-μg g^{-1} levels throughout the value chain, with only minor differences between the four stages.

For two key CEA-Liten value-chain materials (Nd–Pr alloy and Ribbon 3), independent CEA-Liten/supplier data are available for Nd + Pr, total REE (ΣREE) (Table S8), and selected individual REEs (Table S9). For Nd + Pr and ΣREE, this study/CEA-Liten ratios are 0.94 for the Nd–Pr alloy and 1.11 for Ribbon 3, indicating overall agreement at the ≈10–15% level between the two datasets. At the element level, Nd and Pr agree closely between this study and CEA-Liten (≤2% absolute difference). Larger discrepancies are limited to a few trace elements, most notably Sm in the Nd–Pr alloy (Table S9). These outliers are restricted to minor constituents and do not affect the interpretation based on the internally consistent $REE_i/\Sigma REE$ patterns reported here.

Overall, the CEA-Liten value-chain samples maintain similar $REE_i/\Sigma REE$ ratios from alloy to final magnet, with only small variations in trace element levels such as those of Ce, Sm, Gd and Dy. These subtle shifts can be explained by specific contaminations rather than by deliberate modification of the Nd–Pr-dominated REE budget. During strip casting, a minor reaction between the molten alloy and the alumina crucible surface may occur, and residues from previous castings can lead to cross-contamination, causing slight increases in Ce and Dy. In jet-milling, fine dust from prior batches, such as Sm–Co alloys, may remain in hard-to-clean areas, resulting in carry-over contamination of Sm. Finally, during sintering, volatile elements like Dy can evaporate from previously sintered alloys and deposit on furnace walls, later contaminating subsequent magnets. Together, these mechanisms explain the minor shifts observed, confirming that the alloy formulation is largely conserved along the production chain and that most changes in REE composition during manufacturing are second-order.

3.6.4. Ribbons. In addition to the ribbon supplied by CEA-Liten, the study incorporated two commercially procured ribbons, sourced from Japan and Europe, respectively. Fig. 5D illustrates the chondrite-normalized REE patterns for these three ribbons, displayed on a logarithmic scale. As shown in Fig. 5D, the overall trend is a systematic decrease from LREEs to HREEs, accompanied by a pronounced enrichment in Nd and Pr, consistent with the patterns observed in both the magnets and the production chain samples.

Unlike the magnets, the REE patterns of the three ribbons are largely similar, with the ribbon from CEA-Liten displaying the most distinct profile. Eu concentrations are also omitted here, as they remained below the procedural blank in all samples. Among the LREEs, La, Sm and Nd–Pr proportions are broadly comparable across the three ribbons (La ≈ 140–170 μg g^{-1}; Sm ≈ 40–46 μg g^{-1}; Nd ≈ 71–78 wt% of ΣREE; Pr ≈ 17–23 wt% of ΣREE). Ce, however, is clearly more abundant in the CEA-Liten ribbon (Ce ≈ 670 μg g^{-1} relative to the ΣREE) than in the Japanese (≈290 μg g^{-1}) and European ribbons (≈385 μg g^{-1}). The principal exception within the LREE group is Gd, which is elevated in the Japanese ribbon (≈35 μg g^{-1}) compared with the European (≈15 μg g^{-1}) and CEA-Liten ribbons (≈12 μg g^{-1}), while remaining within the μg g^{-1} range.

The most pronounced differences are observed among the HREEs. Tb is strongly enriched in the European ribbon (≈540 μg g^{-1} relative to ΣREE), whereas the Japanese and CEA-Liten ribbons show similarly low Tb levels (≈30 μg g^{-1}). The commercially procured ribbons are also characterized by a strong Dy enrichment, accounting for ≈10–11 wt% of ΣREE in both materials (Table S7). The concentrations of other HREEs (Ho–Lu) are substantially higher in the commercial ribbons than in the CEA-Liten ribbon, with Lu showing the clearest contrast (Japan ≈17 μg g^{-1}; Europe ≈6 μg g^{-1}; CEA-Liten ≈0.04 μg g^{-1}, relative to the ΣREE). Within the commercial pair, the Japanese sample tends to display higher concentrations in the range from Er to Yb, while Y varies comparatively little across all three ribbons (≈4–7 μg g^{-1}; Table S7).

For the two commercially procured ribbons (Ribbon 1, Japan; Ribbon 2, Europe), supplier-reported compositions are available and can be compared with our ICP-MS dataset. At the bulk level (Table S8), slightly higher Nd + Pr and ΣREE values were obtained in this study than in the supplier dataset, with UGent/supplier ratios of 1.08 (Nd + Pr) and 1.07 (ΣREE) for Ribbon 1, and 1.17 (Nd + Pr) and 1.16 (ΣREE) for Ribbon 2. When element-by-element data are reported (Table S9), the major contributors match closely overall (*e.g.*, Ribbon 1: Nd ≈ 71.9 *vs.* 70.7 and Pr ≈ 17.4 *vs.* 17.8, wt% of ΣREE; Dy ≈ 10.6 *vs.* 11.5, wt% of ΣREE), and Ribbon 2 shows a similarly small offset for Dy (≈11.3 *vs.* 12.2, wt% of ΣREE). The main discrepancy is confined to a trace constituent, Tb in Ribbon 2, for which the supplier value (≈1876 μg g^{-1} relative to the ΣREE) exceeds our result (≈541 μg g^{-1}) by a factor of ≈3–4. As in the value-chain comparison, this outlier is restricted to a minor element and does not affect the interpretation based on the internally consistent REE_i/ΣREE patterns discussed here.

The differences between the REE patterns of the ribbons are less pronounced than those observed among the different magnets, although measurable variations occur between commercially procured ribbons. These results indicate that the commercial ribbons share a broadly similar Nd–Pr-dominated base composition, while the contrasting HREE levels suggest differences in intentional HREE additions and/or processing choices, potentially reflecting differences in supplier feedstocks and product specifications. However, REE patterns in manufactured materials are primarily governed by formulation and processing and therefore do not, on their own, allow a robust attribution of upstream raw-material provenance. In line with Fig. 5C, the REE pattern along the CEA-Liten value chain remains largely invariant, supporting limited REE fractionation during the processing steps.

3.7. Comparison of the methodology with existing analytical approaches

The offline two-column separation approach presented here enables accurate REE quantification in Nd–Fe–B magnets using

Table 6 Comparison of analytical methods for REE determination in Nd–Fe–B magnets

Method	Main limitations	Key advantages of the current approach
Direct ICP-MS	Severe Fe matrix effects; polyatomic interferences; poor HREE accuracy	Enables accurate REE quantification using standard quadrupole-based ICP-MS through effective Fe removal and REE pre-separation
ICP-OES	Lower sensitivity; Fe matrix effects; limited HREE accuracy	Achieves higher sensitivity and cleaner spectra after offline separation
Online IC-ICP-MS	Dedicated chromatographic system required; complex optimization; higher cost	Offline workflow avoids the need for specialized equipment and reduces operational complexity
ICP-MS/MS	Reaction/collision gases only partially mitigate polyatomic interferences in a multi-element approach	Interference removal based on sample preparation (physical separation) rather than on chemical resolution during the measurement
Chromatography with TRU/SCX resins	Single-resin retention of all REEs limits HREE resolution and quantification; often requires multiple clean-up steps	Two-column scheme provides sequential Fe removal and REE fractionation, improving HREE accuracy and reproducibility
LA-ICP-MS	Dedicated LA system required; matrix effects; remaining polyatomic interferences; poor HREE accuracy	Offline workflow avoids the need for specialized equipment and allows interference-free analysis

standard quadrupole-based ICP-MS, providing a practical alternative for laboratories without access to high-resolution or tandem ICP-MS (ICP-MS/MS) instrumentation. Compared with other strategies—such as direct ICP-MS, ICP-OES, online ion chromatography (IC) – ICP-MS, ICP-MS/MS with reaction gases, or chromatographic schemes based on TRU or SCX resins—the method offers a favorable balance of analytical performance, robustness, throughput, cost, and operational simplicity.

Direct ICP-MS and ICP-OES suffer from strong Fe-matrix effects and limited HREE accuracy. Online IC-ICP-MS provides excellent interference mitigation but requires dedicated instrumentation and careful optimization of flow, eluent composition, and acquisition parameters to properly resolve chromatographic peaks. ICP-MS/MS with collision or reaction gases cannot combine full resolution of polyatomic interferences with a multi-element approach. High-resolution sector-field ICP-MS instruments do not offer a mass resolution to resolve all spectral interferences caused by the occurrence of oxide and hydroxide ions. Laser ablation ICP-MS avoids sample digestion but, like IC-ICP-MS, requires dedicated instrumentation and is limited by Fe matrix effects and polyatomic interferences, reducing the accuracy of HREE quantification.

In contrast, the approach developed here achieves effective Fe removal and REE separation offline, enabling interference-free analysis with widely accessible equipment. The chromatographic approach used yields enhanced REE resolution compared with TRU or SCX resin-based schemes, which retain all REEs together and therefore restrict accurate determination of HREEs even after Fe removal. The main limitations and key advantages of the current approach are summarized in Table 6.

4. Conclusions

In this study, a method for the determination of REEs in Nd–Fe–B permanent magnets and production chain samples was developed successfully. The method combines sample preparation using AG® MP-1M and LN (100–150 μm) chromatographic resins with ICP-MS analysis. Physical separation proved essential to overcome interference from polyatomic ions, enabling accurate determination of HREEs despite the formation of oxide and hydroxide ions of LREEs present at substantially higher concentrations. High iron concentrations were found to broaden the elution profile of the LREEs, negatively impacting HREE quantification and necessitating Fe removal *via* AG® MP-1M. Quality control using the BHVO-2 reference material and procedural blanks validated the method's reliability, despite some elements being influenced by elevated procedural blanks, leading to slightly low recoveries compared to certified values. Different REE patterns were observed for the three types of magnets analyzed, while the REE patterns of production chain samples showed little variation throughout the manufacturing process, apart from minor shifts in trace REEs that are consistent with contamination and processing-related carry-over rather than changes in the Nd–Pr-dominated REE budget. The commercially procured ribbons share a broadly similar Nd–Pr-dominated base composition, but their HREE signatures differ, indicating variable HREE additions and/or processing choices, consistent with differences in alloy specifications and/or supplier feedstocks. This study carried out within the MaDiTraCe project presents the first comprehensive quantification of REE concentrations in both permanent magnets and associated production chain samples, contributing to the advancement of transparency, traceability, and sustainability in raw material supply chains.

Author contributions

L. S. C.: conceptualization, methodology, validation, formal analysis, investigation, data curation, writing – original draft. C. R.: resources, writing – review & editing. D. L.: resources, writing – review & editing. F. V.: conceptualization, supervision, project administration, writing – review and editing.

Conflicts of interest

There are no conflicts to declare.

Data availability

All data discussed in the paper are included either in the paper itself or in the supplementary information (SI). Supplementary information is available. See DOI: https://doi.org/10.1039/d5ja00513b.

Acknowledgements

This research received funding from the European Union under the MaDiTraCe project (Grant Agreement No. 101091502). The authors thank Noureddine Menad from BRGM and Xuan Liu from GTK for providing magnet samples, the former from the Valomag project (demagnetized at the Plat'Inn platform of BRGM with the support of Maxime Boucheron) and the latter collected during the Nordic Sustainable Minerals project supported by Nordic Innovation. Catherine Guerrot is acknowledged for developing the dissolution protocol, Raphaël Dupuy for sample preparation, and Catherine Lerouge for maintaining the samples under a controlled atmosphere. Daniel Monfort Climent is acknowledged for facilitating contacts.

References

1 V. Balaram, *Geosci. Front.*, 2019, **10**, 1285–1303.
2 M. Hoshino, K. Sanematsu and Y. Watanabe, in *Handbook on the Physics and Chemistry of Rare Earths*, 2016, vol. 49, pp. 129–291.
3 S. L. Liu, H. R. Fan, X. Liu, J. Meng, A. R. Butcher, L. Yann, K. F. Yang and X. C. Li, *Ore Geol. Rev.*, 2023, **157**, 105428.
4 N. Dushyantha, N. Batapola, I. M. S. K. Ilankoon, S. Rohitha, R. Premasiri, B. Abeysinghe, N. Ratnayake and K. Dissanayake, *Ore Geol. Rev.*, 2020, **122**, 103521.
5 L. M. Suli, W. H. W. Ibrahim, B. A. Aziz, M. R. Deraman and N. A. Ismail, *Chem. Eng. Res. Bull.*, 2017, **19**, 20–35.

6 U.S. Geological Survey, *Mineral Commodity Summaries 2024: Rare Earths*, U.S. Department of the Interior, Washington, DC, 2024, pp. 132–133.
7 J. Hackett, E. Sabatino, M. Bint, D. Naradichiantama, M. Gjerstad, J. Bentham, J. Fischbach, L. Bearn and Y. Clavilier, *Critical Raw Materials and European Defence, March 2025. P. Kalvig, MiMa Rapport*, 2022, vol. 1, p. 253.
8 X. P. Meehan, M. Sadan and D. Seng Lawn, *Extr. Ind. Soc.*, 2025, **22**, 101579.
9 P. Kalvig, *MiMa Rapport*, 2022, 1, 253.
10 China's share in rare earth magnet production, 2024, https://www.iea.org/data-and-statistics/charts/china-s-share-in-rare-earth-magnet-production-2024, accessed 16 December 2025.
11 How vulnerable is the euro area to restrictions on Chinese rare earth exports?, https://www.ecb.europa.eu/press/economic-bulletin/focus/2025/html/ecb.ebbox202506_01~44d432008e.en.html, accessed 16 December 2025.
12 B. K. Sovacool, S. H. Ali, M. Bazilian, B. Radley, B. Nemery, J. Okatz and D. Mulvaney, *Science*, 2020, **367**, 30–33.
13 S. M. McLennan, Rare earth elements in sedimentary rocks: influence of provenance and sedimentary processes, *Rev. Mineral. Geochem.*, 1989, **21**, 169–200.
14 B. Zawisza, K. Pytlakowska, B. Feist, M. Połowniak, A. Kita and R. Sitko, *J. Anal. At. Spectrom.*, 2011, **26**, 2373–2390.
15 J. A. Barrat and G. Bayon, *Chemosphere*, 2024, **352**, 141487.
16 N. I. Rousis, I. N. Pasias and N. S. Thomaidis, *Anal. Methods*, 2014, **6**, 5899–5908.
17 Z. Varga, R. Katona, Z. Stefánka, M. Wallenius, K. Mayer and A. Nicholl, *Talanta*, 2010, **80**, 1744–1749.
18 B. Zawisza, K. Pytlakowska, B. Feist, M. Połowniak, A. Kita and R. Sitko, *J. Anal. At. Spectrom.*, 2011, **26**, 2373–2390.
19 I. Wysocka, *Talanta*, 2021, **224**, 121636.
20 K. Nakamura and Q. Chang, *Geostand. Geoanal. Res.*, 2007, **31**, 185–197.
21 R. García Fernández and J. I. García Alonso, *J. Chromatogr. A*, 2008, **1180**, 59–65.
22 B. Hu, M. He, B. Chen and Z. Jiang, in *Handbook of Rare Earth Elements: Analytics*, ed. A. Golloch, De Gruyter, Berlin/Boston, 2017, ch. 3, pp. 14–73.
23 L. M. Arrigo, J. Jiang, Z. S. Finch, J. M. Bowen, C. L. Beck, J. I. Friese, L. R. Greenwood and B. N. Seiner, *J. Radioanal. Nucl. Chem.*, 2021, **327**, 457–463.
24 Material & Digital Traceability for CRM Certification, https://www.maditrace.eu, accessed 1 August 2025.
25 P. Fernández, F. Sánchez, M. Mavroudi, K. Ungerer, P. Hartlieb and M. Tost, *Berg- Huettenmaenn. Monatsh.*, 2025, **170**, 81–87.
26 L. Van Heghe, O. Deltombe, J. Delanghe, H. Depypere and F. Vanhaecke, *J. Anal. At. Spectrom.*, 2014, **29**, 478–482.
27 M. Costas-Rodríguez, Y. Anoshkina, S. Lauwens, H. Van Vlierberghe, J. Delanghe and F. Vanhaecke, *J. Anal. At. Spectrom.*, 2015, **30**, 491–498.
28 M. Kaya, *Curr. Opin. Green Sustainable Chem.*, 2024, **46**, 100884.
29 X. Liu, J. Kløve Keiding, N. Coint, E. Jonsson *et al.*, *Mineral to Metal Traceability: A Proof-Of-Concept Study of Rare Earth Elements in the Nordic Region*, Nordic Council of Ministers, Nordic Innovation, Oslo, 2024, p. 91.
30 Eichrom Technologies LLC, *LN Resin*, Eichrom, https://www.eichrom.com/products/ln-resins/, accessed May 6, 2025.
31 K. L. Nash and M. P. Jensen, *Sep. Sci. Technol.*, 2001, **36**, 1257–1282.
32 A. M. Shahr El-Din, H. E. Rizk, E. H. Borai and E. S. M. El Afifi, *Chem. Pap.*, 2023, **77**, 2525–2538.
33 C. Pin, M. Lancelot and J. F. Poitrasson, *Anal. Chim. Acta*, 1996, **339**, 79–89.
34 United States Geological Survey, *Reference Material Information Sheet: BHVO-2 (Hawaiian Volcano Observatory Basalt)*.
35 W. F. McDonough and S.-s. Sun, The composition of the Earth, *Chem. Geol.*, 1995, **120**(3–4), 223–253.
36 X. Yang, Y. Zheng, X. Y. Yang, M. J. Le Bas, *et al.*, A Geochemical Study of an REE-rich Carbonatite Dyke at Bayan Obo, Inner Mongolia, Northern China, *Acta Geol. Sin.*, 2010, **74**(3), 605–612.
37 J. Dostal and G. Ochir, Rare Earth Element Deposits in Mongolia, *Minerals*, 2023, **13**(1), 129.
38 D. Losno, M. Dèzes, C. Guerrot, A.-M. Desaulty, C. Rado and F. Vanhaecke, *23rd Swiss Geoscience Meeting*, Bern, 2025.

